

## COMPARISON OF THE 1998 APRIL 29 M6.8 AND 1998 NOVEMBER 5 M8.4 FLARES

HAIMIN WANG, PHILIP R. GOODE, CARSTEN DENKER, GUO YANG, AND VASYL YURCHISHIN  
Big Bear Solar Observatory, New Jersey Institute of Technology, 40386 North Shore Lane, Big Bear City, CA 92314-9672; haimin@solar.njit.edu

NARIAKI NITTA

Lockheed Martin Solar and Astrophysics Laboratory

JOSEPH B. GURMAN

NASA Goddard Space Flight Center

CHRIS ST. CYR

Computational Physics, Incorporated, Naval Research Laboratory

AND

ALEXANDER G. KOSOVICHEV

W. W. Hansen Experimental Physics Laboratory, Stanford University

Received 1999 September 9; accepted 2000 January 24

### ABSTRACT

We combined, and analyzed in detail, the  $H\alpha$  and magnetograph data from Big Bear Solar Observatory (BBSO), full-disk magnetograms from the Michelson Doppler Imager (MDI) on board *Solar and Heliospheric Observatory (SOHO)*, coronagraph data from the Large Angle Spectrometric Coronagraph (LASCO) of *SOHO*, Fe XII 195 Å data from the Extreme ultraviolet Imaging Telescope (EIT) of *SOHO*, and *Yohkoh* soft X-ray telescope (SXT) data of the M6.8 flare of 1998 April 29 in National Oceanic and Atmospheric Administration (NOAA) region 8375 and the M8.4 flare of 1998 November 5 in NOAA region 8384. These two flares have remarkable similarities:

1. Partial halo coronal mass ejections (CMEs) were observed for both events. For the 1998 April 29 event, even though the flare occurred in the southeast of the disk center, the ejected material moved predominantly across the equator, and the central part of the CME occurred in the northeast limb. The direction in which the cusp points in the postflare SXT images determines the dominant direction of the CMEs.
2. Coronal dimming was clearly observed in EIT Fe XII 195 Å for both but was not observed in *Yohkoh* SXT for either event. Dimming started 2 hr before the onset of the flares, indicating large-scale coronal restructuring before both flares.
3. No global or local photospheric magnetic field change was detected from either event; in particular, no magnetic field change was found in the dimming areas.
4. Both events lasted several hours and, thus, could be classified as long duration events (LDEs).

However, they are different in the following important aspects. For the 1998 April 29 event, the flare and the CME are associated with an erupting filament in which the two initial ribbons were well connected and then gradually separated. SXT preflare images show the classical S-shape sheared configuration (sigmoid structure). For the 1998 November 5 event, two initial ribbons were well separated, and the SXT preflare image shows the interaction of at least two loops. In addition, no filament eruption was observed. We conclude that even though these two events resulted in similar coronal consequences, they are due to two distinct physical processes: eruption of sheared loops and interaction of two loops.

*Subject headings:* Sun: corona — Sun: flares — Sun: magnetic fields

### 1. INTRODUCTION

A solar coronal mass ejection (CME) represents a large-scale rearrangement of the Sun's magnetic structure that can lead to a coronal transient in the interplanetary medium. Each CME may carry away a mass of up to  $10^{13}$  kg and release up to  $10^{25}$  J of energy from the coronal magnetic fields (Harrison 1991, 1994, 1995). CMEs have been studied using a number of coronagraphs since the 1970s, e.g., *Skylab*, *Solwind*, and *Solar Maximum Mission (SMM)*. Filament eruptions and solar flares may be local events that are associated with CMEs; however, the connection remains to be established. As a matter of fact, most observations failed to establish a systematic correlation among the onset of solar flares, prominence eruptions, and CMEs (Verma 1990; Feynman & Hundhausen 1994; Harrison 1995; McAllister et al. 1996; Yang & Wang 1999). One

of the difficulties in establishing a possible relationship between filament eruptions and CMEs is that CMEs are more likely to be detected if they are limb events, while filament eruptions are more easily visible as disk events. Any search for a correlation between filament eruptions and CMEs needs to be able to consider both disk and limb CMEs and their attendant phenomena. The launch of a new generation coronagraph—the Large Angle Spectroscopic Coronagraph (LASCO) on board *Solar and Heliospheric Observatory (SOHO)*; Domingo, Fleck, & Poland 1995)—provides the most advanced tool for studying the dynamics of coronal structure (Brueckner et al. 1995). LASCO comprises three coronagraphs (C1, C2, and C3), extending from 1.1 to 30 solar radii. The white-light instruments (C2 and C3) not only provide excellent observations of limb CME events, but also have the sensitivity to detect the “halo”

from the disk events after the CME material moves beyond the edge of the occulting disk. Halo events (including “partial” halo events) are related to the Earth-directed CMEs, and the first of this kind of event was reported by Howard, Michels, & Sheeley (1982) using observations made with the Solwind coronagraph on the *P78-1* spacecraft. Several halo events have been reported by LASCO (Plunkett et al. 1998; Thompson et al. 1998; Zarro et al. 1999); two additional events are studied in this paper.

Disk coronal dimmings have been detected recently in association with halo events detected with the *Yohkoh* soft X-ray telescope (SXT; Tsuneta et al. 1991) and *SOHO* Extreme ultraviolet Imaging Telescope (EIT; Delaboudinière et al. 1995); see, e.g., Gopalswamy & Hanaoka (1998), Sterling & Hudson (1997), and Thompson et al. (1998). One interpretation is that those transient dimmings track the loss of the coronal mass that is swept into the CMEs.

At the end of 1995, Big Bear Solar Observatory (BBSO) started its new generation of full-disk H $\alpha$  observations. Every minute, a full-disk H $\alpha$  image is recorded by a 2048  $\times$  2048 Kodak 8 bit Megaplus camera with the 8 inch Singer-Link telescope. The pixel size of the images is roughly 1”, which yields a spatial resolution of 2”. Because of BBSO’s long-lasting clear skies and good seeing conditions, these movies provide a unique tool for monitoring filaments continuously during their disk passage. Daily LASCO and EIT MPEG movies are now on-line, facilitating the comparison with BBSO movies. In addition, high-resolution H $\alpha$  and magnetograph movies provide important information on the morphology of active regions and flares.

In this paper, we present comprehensive data sets of two M-class flares and associated CMEs by combining data from BBSO, *SOHO*, and *Yohkoh*. We will briefly describe first the observations, then the differences and similarities between the two events, and finally we will present discussions of the physics of these two events deduced from our observations.

## 2. OBSERVATIONS AND DATA REDUCTION

The two flares under discussion are the only upper M-class events in our data archive that had complete coverage in BBSO (H $\alpha$  and magnetograms), LASCO, Michelson Doppler Imager (MDI), EIT, and SXT. Table 1 lists the basic properties of the flares.

### 2.1. *SOHO* Observations

The data we analyzed are from three of the payload instruments of *SOHO*:

1. LASCO coronagraph data. We were especially interested in the C2 and C3 white-light data for CMEs. C2 and C3 are two externally occulted instruments. C2 covers the range of 2–6 solar radii and C3, 4–32 solar radii (Brueckner et al. 1995). The cadence for our data was between 30 and 90 minutes.

2. Full-disk MDI magnetograms. MDI mainly obtains full-disk Dopplergrams, for the investigation of solar oscillation. However, it can obtain magnetograms with various cadence and image size (Scherrer et al. 1995). For the data used in the current study, the cadence was 90 minutes and the pixel size was 2”.

TABLE 1  
PARAMETERS OF TWO FLARES

Flare	1998 Apr 29	1998 Nov 5
Start time (UT).....	1606	1900
Peak time (UT).....	1637	1955
X-ray class .....	M6.8	M8.4
Disk location .....	S18 E20	N22 W18
Two-ribbon .....	Yes	Yes
Filament eruption.....	Yes	No
CME .....	Partial halo	Partial halo

3. EIT Fe XII 195 Å full-disk movies. EIT provides wide-field images of the corona and transition region on the solar disk and up to 1.5 solar radii above the solar limb. It observes in four spectral lines: Fe IX (171 Å), Fe XII (195 Å), Fe XV (284 Å), and He II (304 Å). These lines allow imaging of solar plasmas at certain temperature diagnostics in the range  $6 \times 10^4$  to  $3 \times 10^6$  K (Delaboudinière et al. 1995). For the two events discussed in this paper, only Fe XII 195 Å data were obtained continuously. The sensitivity of this line peaks between 1 and 2 MK. Cadence was 15 minutes to 1 hr, and pixel resolution was 2”.5.

### 2.2. *BBSO* Observations

1. Full-disk H $\alpha$  movies. The cadence was 1 minute and the pixel resolution was 1”. The observations covered both events completely.

2. High-resolution H $\alpha$  observations. They were obtained by the 65 cm reflector, with a 0.25 Å Zeiss filter and an Orbiting Solar Lab (OSL) 12 bit camera. The cadence was 30 s, pixel resolution 0”.3. This observation covered the 1998 November 5 event completely; however, it missed the start and the peak of the 1998 April 29 event.

3. High-resolution line-of-sight magnetograms, obtained by the 25 cm refractor. The pixel resolution was 0”.5, and cadence 30 s. The integration time of each image was 4 s.

### 2.3. *Yohkoh/SXT* Observations

SXT is an instrument on board *Yohkoh* for studying the thermal structure of solar plasma (Tsuneta et al. 1991). For the two events analyzed in this paper, full-disk *Yohkoh* SXT images were obtained in three filters (A11, A12, and AlMg, which cover a wide temperature range from 3 to 10 MK). Only partial frame images were obtained during the flares. We used standard SXT tools to decompress the images. The cadence during those two flares was 10 minutes to 1 hr. Our analyses concentrated on the A11 filter data, which covers the lower temperature range (about 3 MK), so they can be compared with the EIT 195 Å images more easily. The pixel size of SXT images was 5”. The 1998 April 29 observation was in a nominal mode, while the 1998 November 5 observation was during a CCD bakeout period, so the data had poorer quality.

### 2.4. *Image Alignment*

To compare data from several instruments, data alignment is extremely important. For this particular study, the alignment is relatively easy, as BBSO H $\alpha$ , *SOHO* EIT/MDI/LASCO, and *Yohkoh* SXT images were all full-disk data. Alignment among these images was easily done by limb

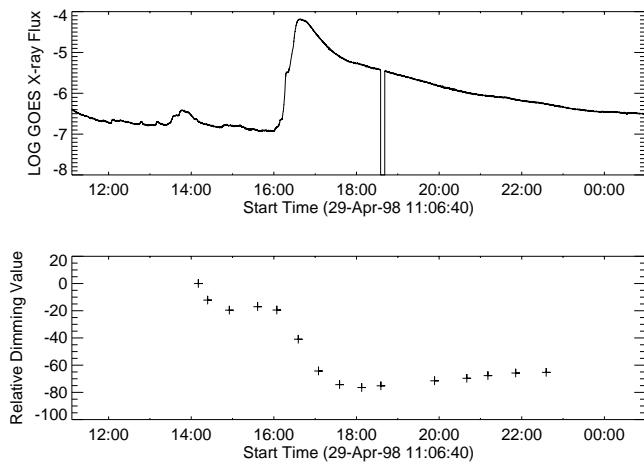


FIG. 1.—*Top*: GOES X-ray time profile of 1998 April 29 flare. *Bottom*: EUV dimming of the flare. The value is the contrast integrated over the entire dimming area, in units of  $10^{17}$  cm<sup>2</sup>.

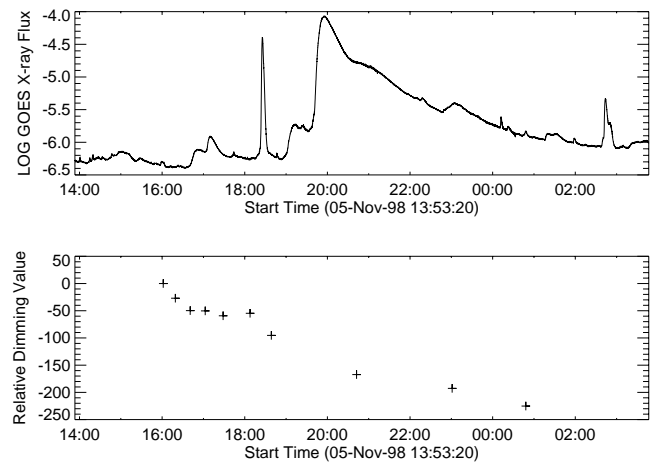


FIG. 2.—*Top*: GOES X-ray time profile of 1998 November 5 flare. *Bottom*: EUV dimming of the flare. The value is the contrast integrated over the entire dimming area, in units of  $10^{17}$  cm<sup>2</sup>.

fitting. Then, the BBSO high-resolution H $\alpha$  images were aligned with BBSO full-disk H $\alpha$  images, and BBSO high-resolution magnetograms were aligned with MDI full-disk magnetograms. Movies were compiled and viewed for all the observing sequences. We believe that the accuracy of image alignment is better than 5". The roll-angle correction (relative rotation of images) is better than 1°; they were detected by manually flicking two full-disk images.

### 3. RESULTS

#### 3.1. Flares

The upper panels of Figures 1 and 2 show GOES soft X-ray 1–8 Å flux plots of the 1998 April 29 and 1998 November 5 flares as a function of time. Clearly, both are long-duration events, lasting several hours. Lower panels show the time plots of the coronal dimming, which will be discussed later.

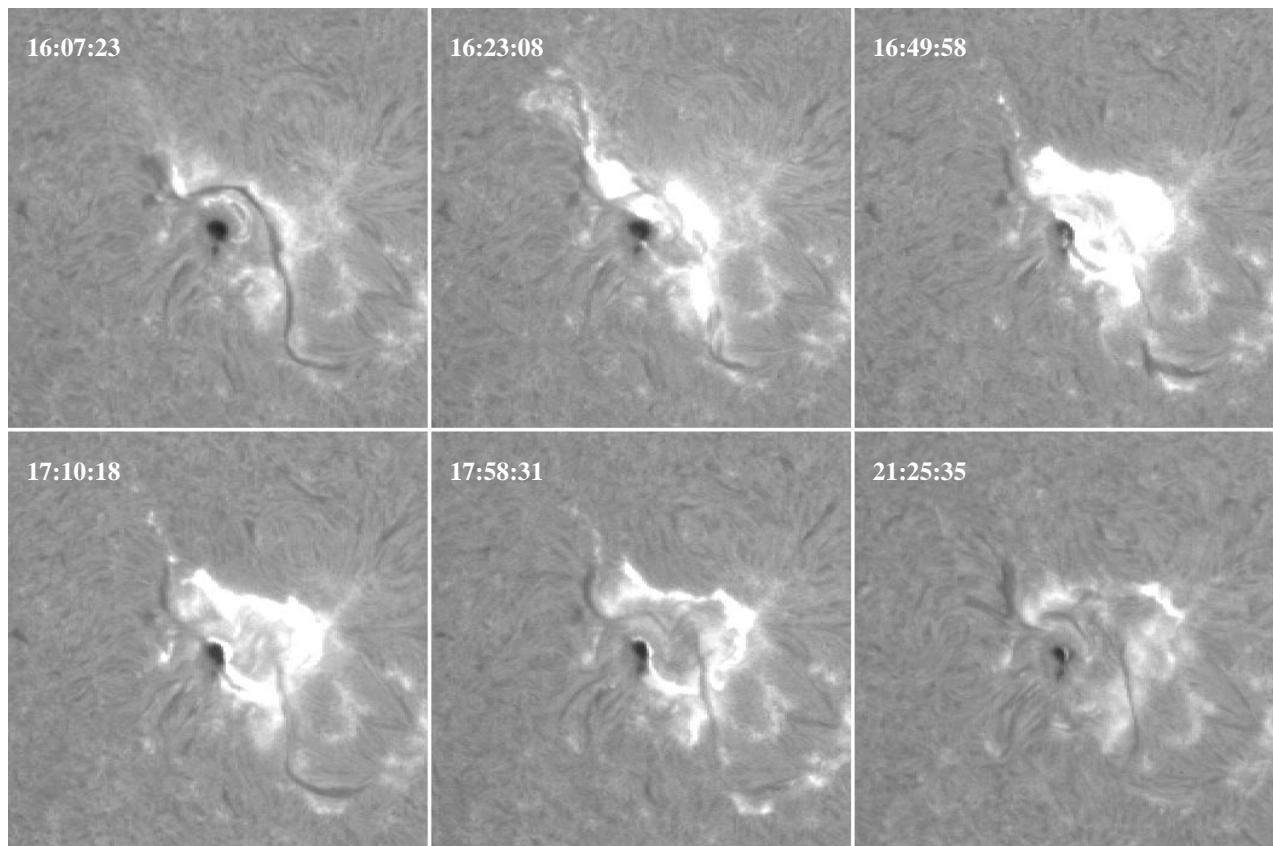


FIG. 3.—Time sequence of H $\alpha$  images of 1998 April 29. The images are from full-disk data; the field of view is 400" by 400".

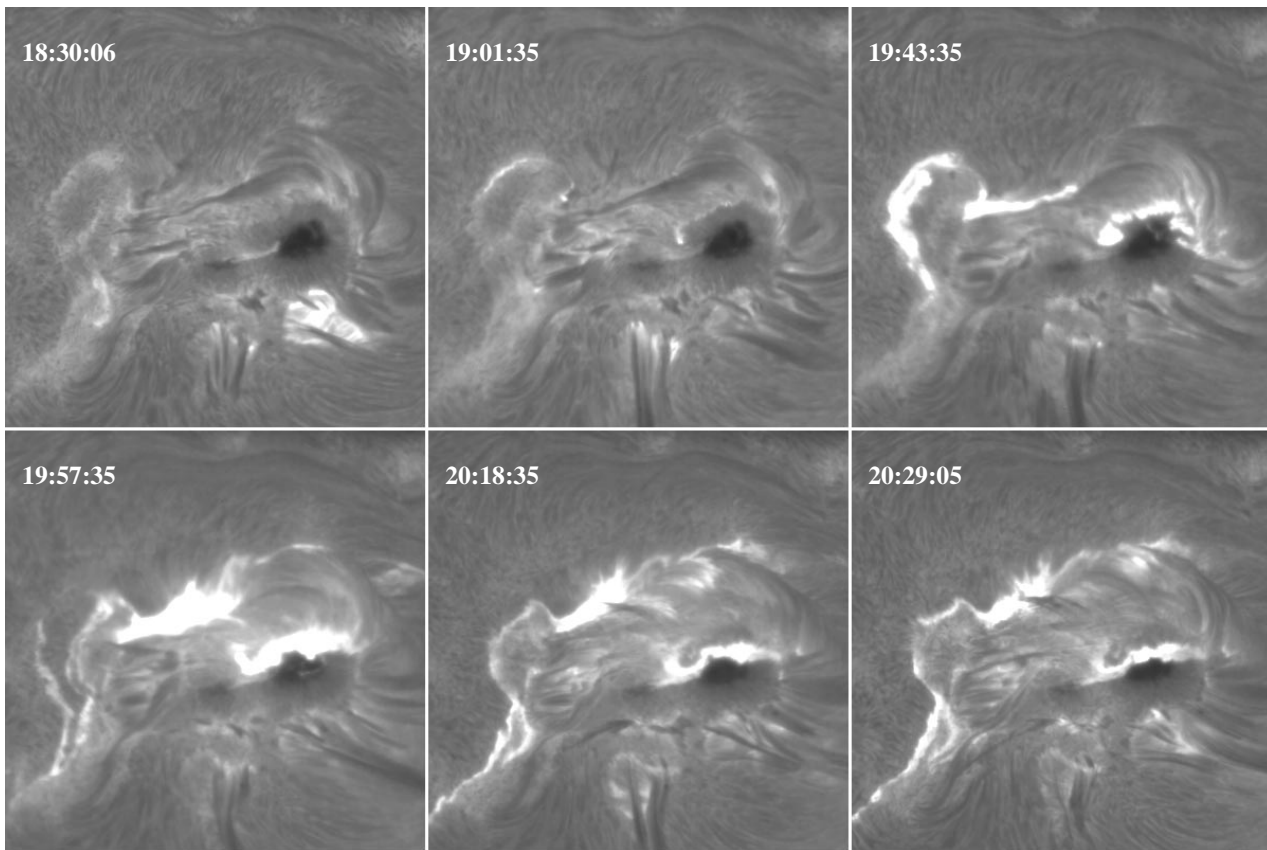


FIG. 4.—Time sequence of H $\alpha$  observations of 1998 November 5. The images are from 65 cm telescope; the field of view is 200" by 200".

Figure 3 shows the development of the 1998 April 29 M6.8 flare in H $\alpha$ . Filament disappearance is clearly associated with this two-ribbon flare. Two initial flare ribbons were very close (barely separable) and moved apart gradually. Only the center section of the filament disappeared during the flare. This event fits nicely with the sigmoid classification of erupting filaments and flares as proposed recently by Canfield, Hudson, & McKenzie (1999).

Figure 4 shows the development of the 1998 November 5 M8.4 flare in H $\alpha$ . This is also a two-ribbon flare; however, there is no filament disappearance, in fact, no filament was present in this active region for the whole period that the region was on the disk. The images are from BBSO high-resolution observations. The two flare ribbons were well separated initially and moved further apart as the flare progressed.

Figures 5 and 6 show the longitudinal magnetic contours overlaid on the flare ribbons at the peaks of the 1998 April 29 and 1998 November 5 events, respectively. Note that the two events are very similar in the sense that the magnetic neutral lines divide two polarities—one side includes a large sunspot, the other side includes just plage regions—and both show two ribbons. For the April 29 event, both ribbons are close to the neutral line; for the November 5 event, the ribbon corresponding to the positive magnetic polarity is close to the neutral line, and the opposite ribbon is farther away.

### 3.2. The Partial Halo CMEs

Figure 7 shows the time sequence of LASCO C2 images of 1998 April 29, with the image that was taken at 1527 UT

subtracted from each, in order to highlight the coronal changes. Note that even though the flare and filament eruption occurred in the southeast part of the disk, the halo CME showed maximum intensity and extension in the northeast limb. We are convinced that the flare and the CME are related, since, in the H $\alpha$  movie,<sup>1</sup> filamentary materials are observed moving across the equator in the direction of the center line of CME, as seen in the LASCO movie. It is hard to demonstrate this motion through other methods. The motion of dark material occurred around 1635 UT, toward the top left. The speed was about 100 km s<sup>-1</sup>.

The CME first appears in C2 as a very bright, flattened mound in the northeast at 1658 UT. There were clear extensions of this mound extending above the poles and into the west, surrounding the occulting disk. The leading edge of the CME traveled through the C2/C3 fields with a constant speed of 1020 km s<sup>-1</sup>. As this mass ejection moved outward, the sides of the mound appeared to travel faster than the center, distorting the original mound with increasing altitude. This is an example of a highly structured halo CME. At 1858 UT, bright linear structured material, interpreted as filamentary fragments, appeared in the northeast and traveled slowly (110 km s<sup>-1</sup>) out of the field of view, consistent with the speed of H $\alpha$  filamentary material observed on the disk.

Figure 8 shows a LASCO C3 image of 1998 November 5, taken 2 hr after the flare at 2330 UT, with the 1649 UT

<sup>1</sup> The H $\alpha$  movie can be viewed at <http://solar.njit.edu/haimin/ha980429.mpg>.

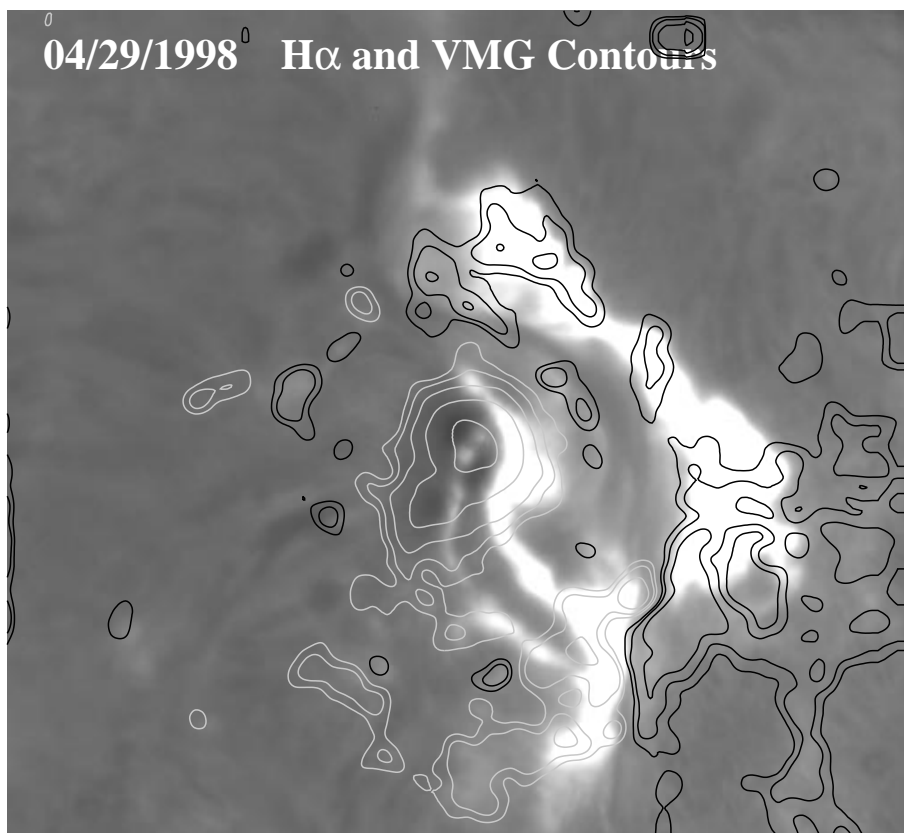


FIG. 5.—H $\alpha$  image at the peak of the flare of 1998 April 29, superposed on a smoothed magnetogram. White contours are positive fields, and black contours are negative fields. Contour levels are 100, 200, 400, and 800 gauss.

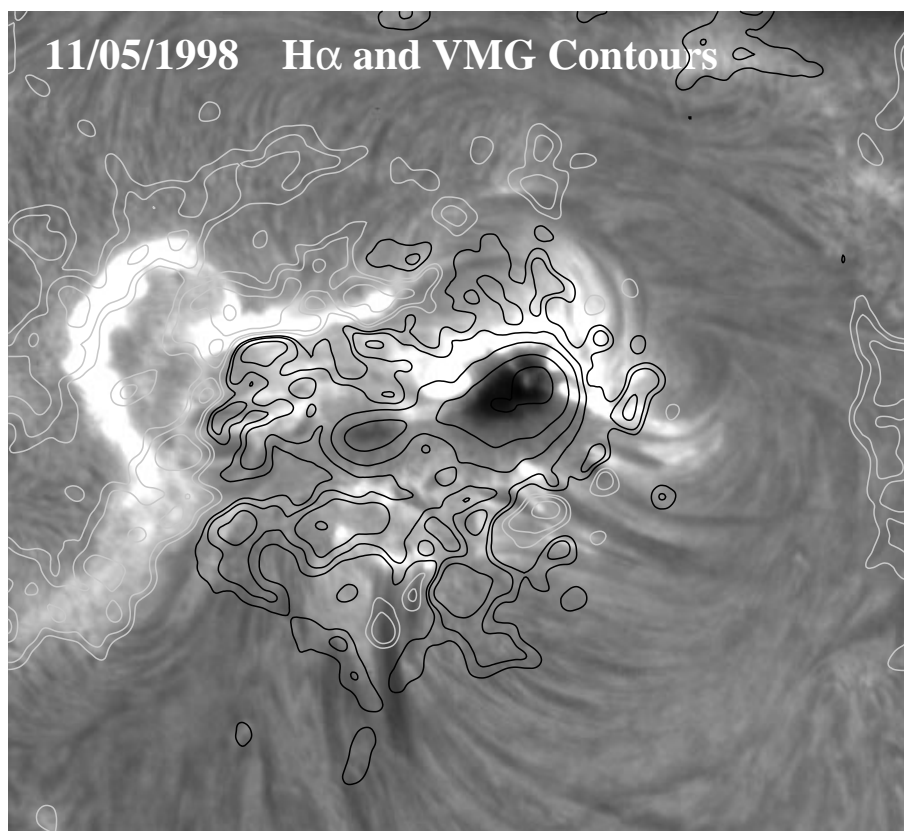


FIG. 6.—H $\alpha$  image at the peak of the flare of 1998 November 5, superposed on a smoothed magnetogram. White contours are positive fields, and black contours are negative fields. Contour levels are 100, 200, 400, and 800 gauss.

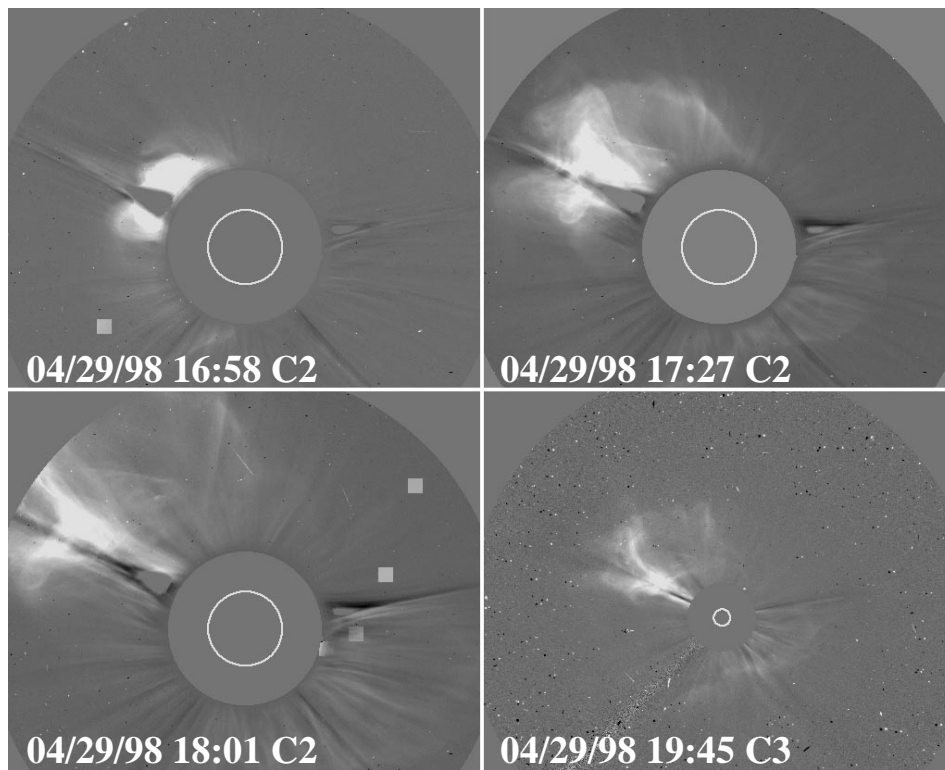


FIG. 7.—Sequence of LASCO C2 images subtracted from a reference image at 1542 UT. Top is north and left is east, the same for all the figures in this paper.

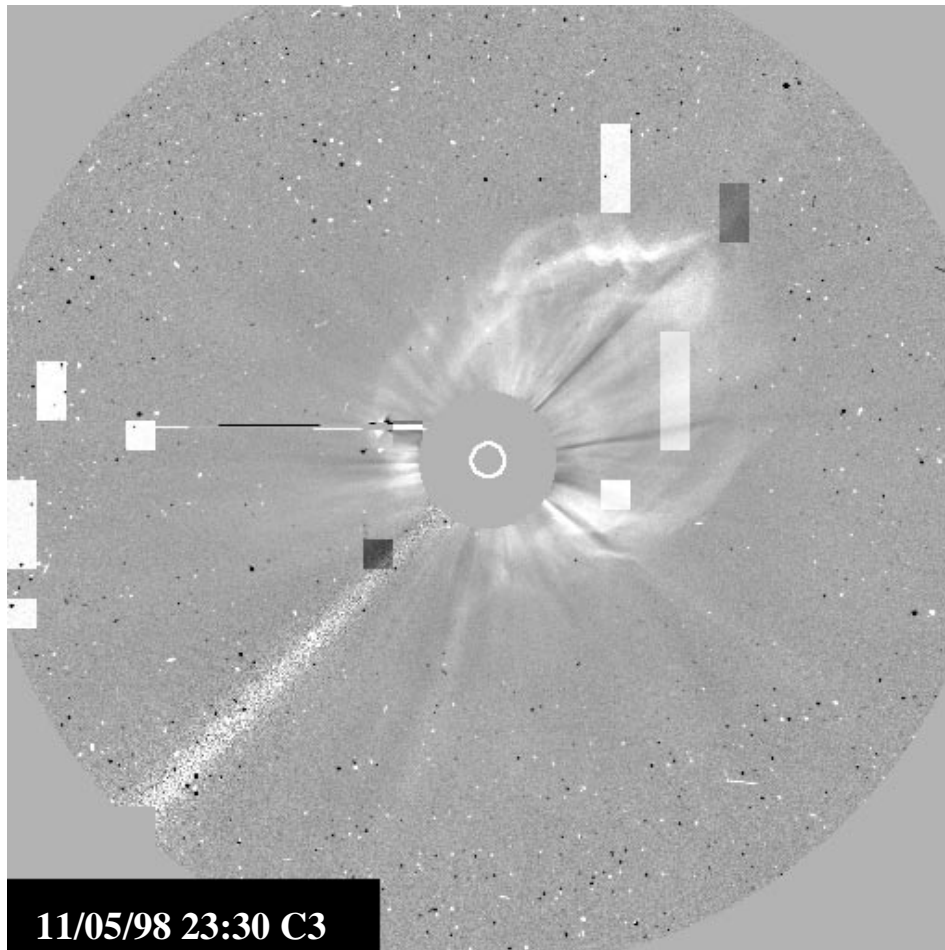


FIG. 8.—LASCO C3 image at 2330 UT subtracted from a reference image at 1649 UT

image, taken 4 hr before the flare, subtracted from it. This event is likely associated with the flare, since the concentration of the CME is in the direction of the northwest limb, and the flare occurred close to that part of the limb. However, we need to be cautious that the CME source region is commonly much larger than the active region, which can be on one side of a CME (Harrison 1995).

The CME first appears in C2 as a bright mound with some internal structure in the northwest at 2033 UT. Faint extensions of the mound can be detected completely surrounding the occulting disk, offset to the northwest. The mass ejection traveled through the C2/C3 fields with an apparent constant speed of  $1155 \text{ km s}^{-1}$  for the leading edge. There is also an apparent deflection of an existing streamer around the mound (to the north-northwest).

To estimate the onset time of the CME is difficult, as we know that CMEs may be accelerated while moving out. So their speeds would be between  $100$  and  $1000 \text{ km s}^{-1}$  when traveling between the surface source and the first appear-

ance on C2. That would give us a 0.5–5 hr delay between the onset and the first appearance on C2. The uncertainty is too big to give an accurate estimate of the onset time of the CME.

### 3.3. Coronal Dimming

Coronal dimmings associated with CMEs have recently received considerable attention. They are observed with *Yohkoh* SXT as both disk events (Sterling & Hudson 1997) and limb events (Gopalswamy & Hanaoka 1998). Thompson et al. (1998) also discovered dimming in EUV associated with CMEs from EIT/*SOHO* observations. Dimmings were also reported using the Coronal Diagnostic Spectrometer (CDS) on *SOHO* (Harrison 1997). For the two events in the current paper, we have the opportunity to study dimming simultaneously with SXT and EIT observations.

The top row of Figure 9 shows EIT  $195 \text{ \AA}$  images before the flare (1920 UT) and after the flare (1953 UT) and the difference between two. Three dimming regions are marked

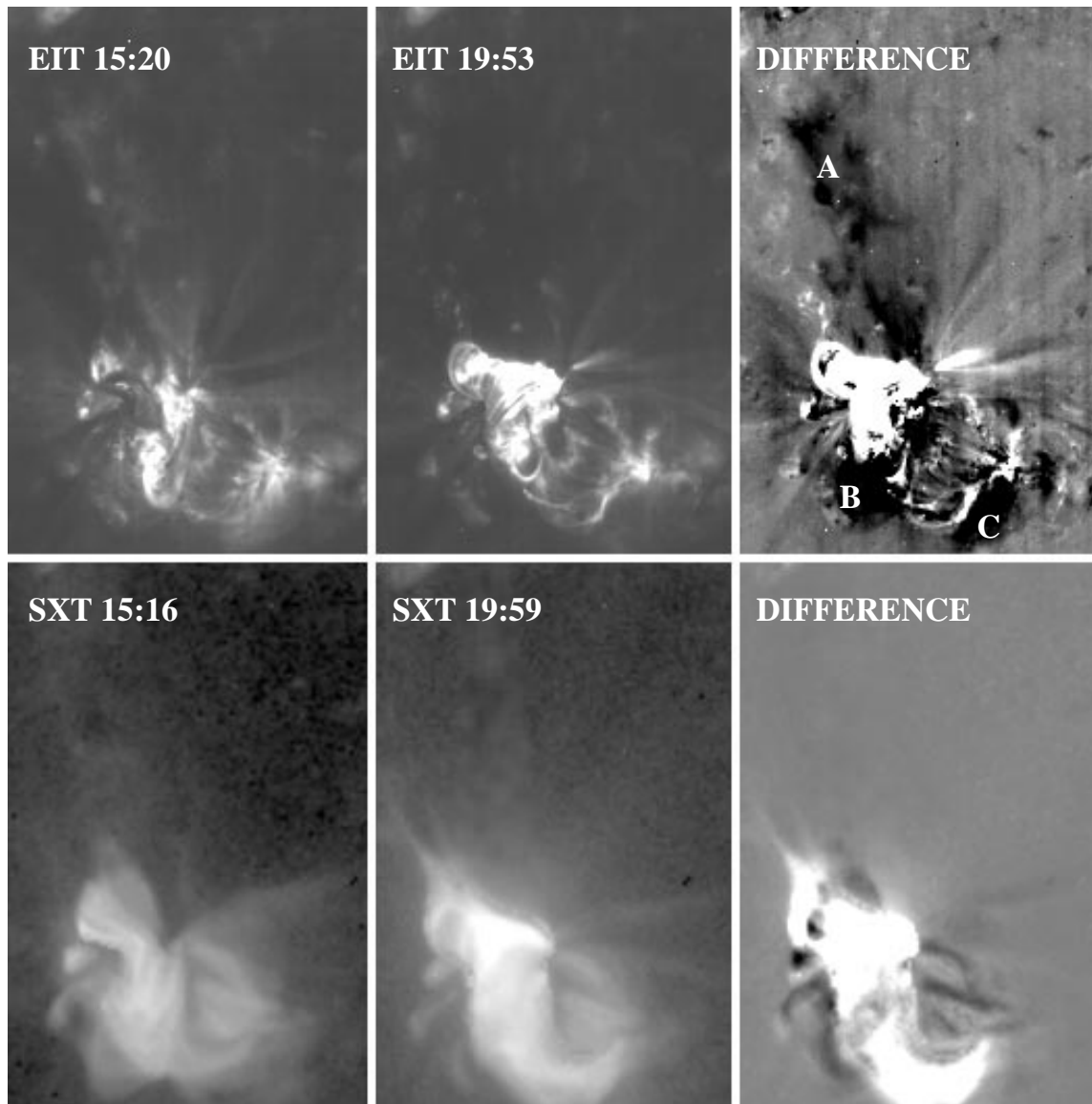


FIG. 9.—*Top row:* pre- and postflare EIT  $195 \text{ \AA}$  images and the difference, showing the EUV dimming associated with the 1998 April 29 flare/CME. Three dimming regions are marked by “A,” “B,” and “C.” *Bottom row:* pre- and postflare SXT images and the difference, showing the lack of corresponding dimming. The field of view is  $350''$  by  $530''$ .

by “A,” “B,” and “C” in the difference image. Note that A is in the general direction in which the CME moves across the disk, toward the limb. The bottom row shows preflare and postflare and the difference between the SXT images. It is somehow surprising that coronal dimming was not observed by the soft X-ray observations, as seen in the lower right panel of Figure 9. The most obvious explanation is the temperature of the lost material: 195 Å emission is formed at a temperature around 1.5 million K, and SXT observations are in the range between 2 and 4 million K. So the ejected material is probably mostly cooler than SXT can see. It also provides a hint that dimming is probably due to a loss in density instead of a decrease in the temperature, as noted by Thompson et al. (1998). Otherwise, SXT dimming would be observed as the coronal material becomes cooler.

Figure 10 shows a similar comparison for the dimming of the 1998 November 5 event. Again, the EIT 195 Å dimming is very extensive, while dimming in SXT is not visible. The primary dimming is in a large area south and southwest of the active region and is marked by six areas (“A” through “F”).

Figures 9 and 10 also demonstrate that the direction of cusp-pointing in SXT postflare images determines the dominant direction of CMEs. For the 1998 April 29 event, it is northeast, and for the 1998 November 5 event, it is northwest. Of course, two examples do not provide statistical meaning in this regard.

In the lower panels of Figures 1 and 2, we plot the relative dimming value in Fe XII 195 Å as a function of time. The value is defined as contrast integrated over all the dimming areas (“A,” “B,” and “C” for the 1998 April 27 event and “A” through “F” for the 1998 November 5 event). For both events, dimming started about 2 hr before the onset of the flares, indicating that a large-scale restructuring started before the flares. It is interesting to note that, for the November 5 event, the rising part of dimming covers three flares, M8.4 and two smaller events before it. The two smaller events occurred in the same active regions but are associated with different magnetic neutral lines. An impulsive M2 flare occurred at 1830 UT and is shown in the first panel of Figure 1 (lower right part of the field of view). It corresponds to the foot of dimming area “E” in Figure 10. A very small C2 flare occurred at 1920 UT; it had extended but very weak brightening over the entire active region.

As we did not have multiwavelength EIT data to derive the temperature and density of dimming plasma, it is hard to derive the mass of lost material. However, we note that our dimming area is in the same order of magnitude as the event studied by Sterling & Hudson (1997), i.e.,  $10^{20}$  cm<sup>2</sup>. If we adopt their calculation, the dimming mass loss is about  $10^{14}$  g. This number is 1–2 orders of magnitude smaller than the mass of a typical CME (Harrison 1994, 1995). Therefore, dimming can count for only a fraction of the mass in a CME.

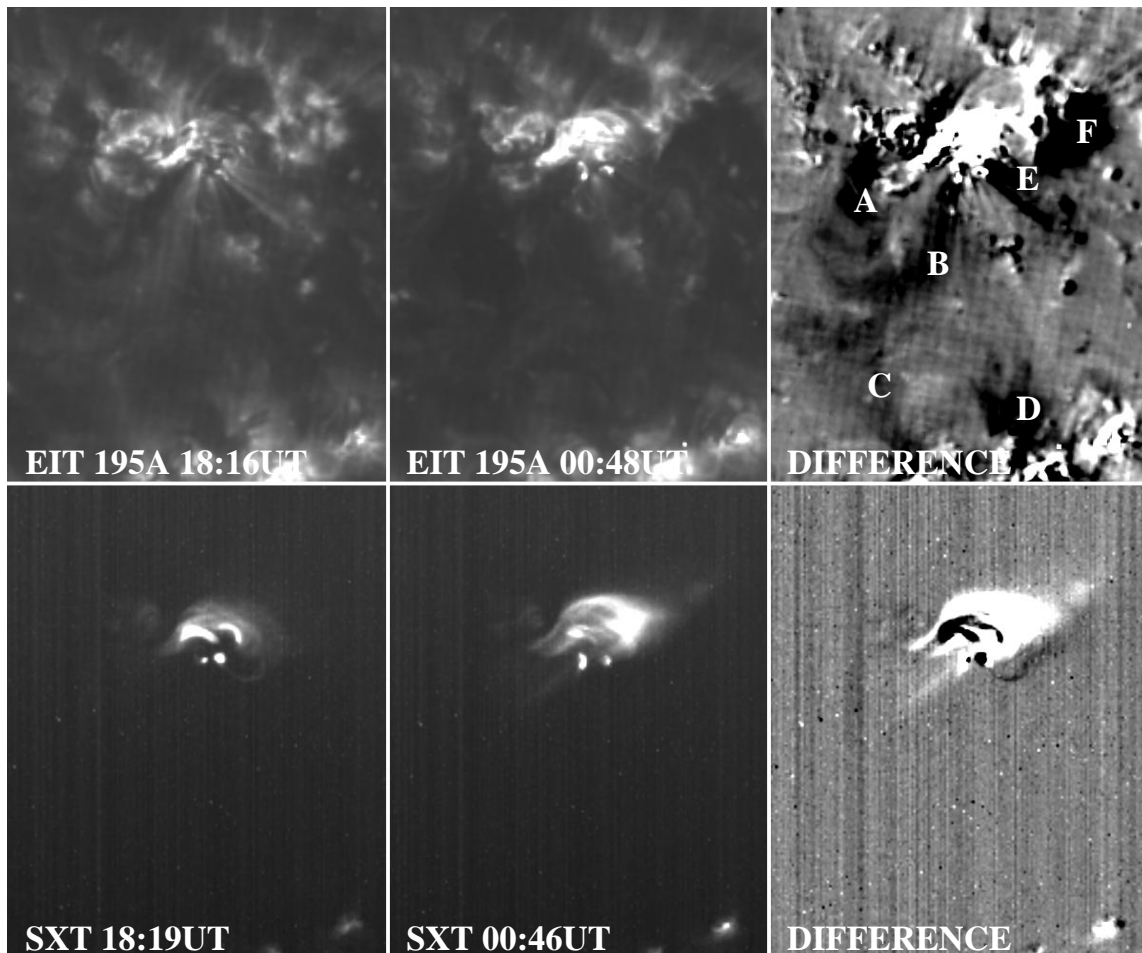


FIG. 10.—Top row: pre- and postflare EIT 195 Å images and the difference, showing the EUV dimming associated with the 1998 November 5 flare/CME. Bottom row: pre- and postflare SXT images and the difference, showing the lack of corresponding dimming. The field of view is 580" by 1000".

### 3.4. Structure and Evolution of Magnetic Fields

Even though the scale of magnetic fields associated with flares and CMEs is not yet clear, it is believed that magnetic fields in the corona change their structure substantially after a major CME/flare event. In the flaring region, it is obvious from the  $H\alpha$  observations that the chromospheric fibril structure changes from a low-lying sheared configuration to higher potential-like postflare loops in both cases. However, it is unclear whether such a major change would show some signal in the photospheric magnetic fields and what the structure of these new coronal holes would be as a result of the dimming. We used BBSO high-resolution magnetograms and MDI/*SOHO* full-disk magnetograms to search

for the answer. EIT and SXT images also show substantial changes in coronal morphology. As demonstrated in Figure 9 for the 1998 April 29 event, the S-shaped sheared roped structure is obvious in the SXT preflare image. It forms a cusp and more of a potential configuration in the postflare SXT image. Postflare loops are also visible in the EIT postflare image. For the 1998 November 5 event, SXT images (Fig. 10) strongly suggest that two interacting loops are visible before the flare and show a high loop after the flare. In order to demonstrate that more clearly, we magnify SXT images and plot them in Figure 11. SXT contours are plotted over by simultaneous magnetograms, one before and one after the flare. Two loops appear to interact near

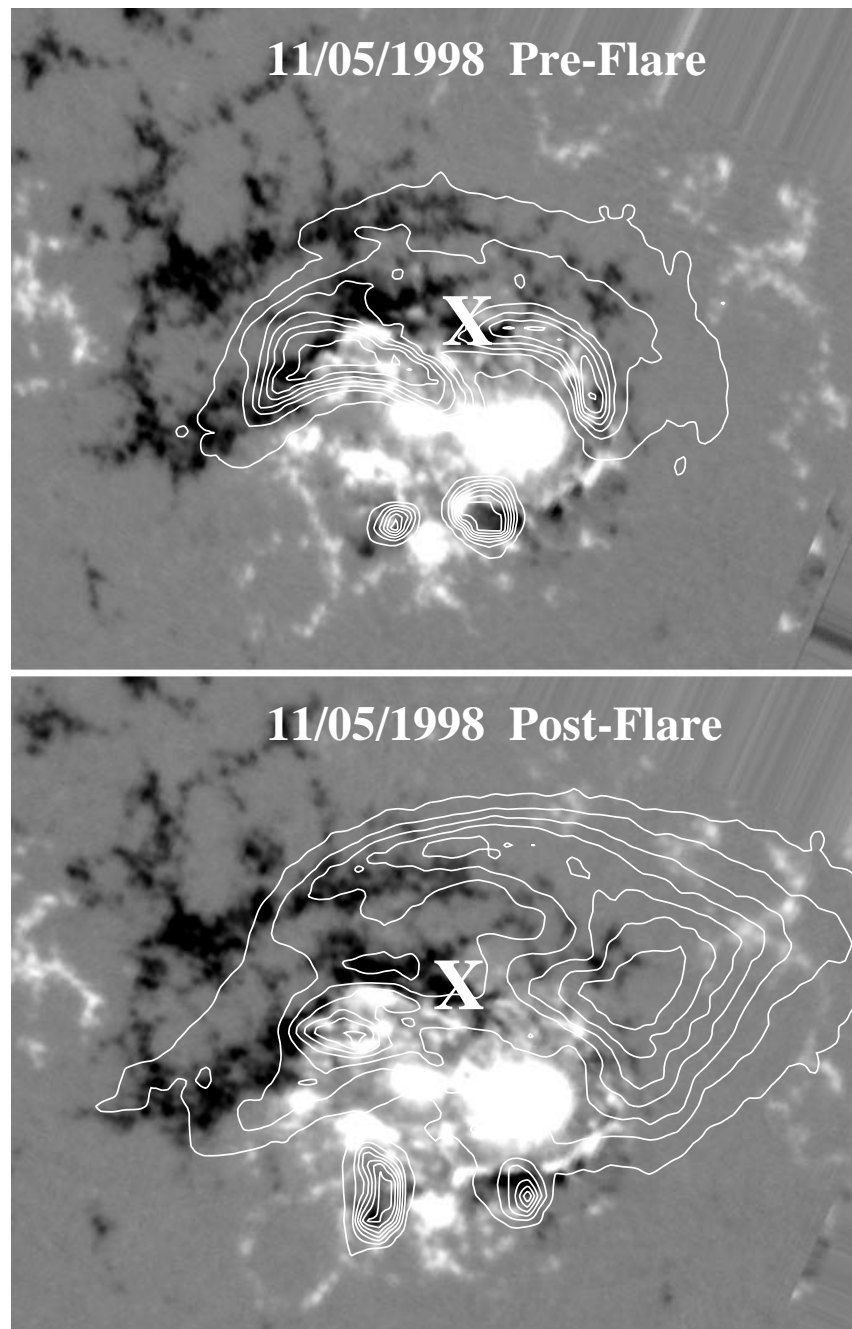


FIG. 11.—SXT contours superposed on corresponding magnetograms on 1998 November 5. The upper panel is the preflare image at 1818 UT, and the lower panel is the postflare image at 2258 UT.

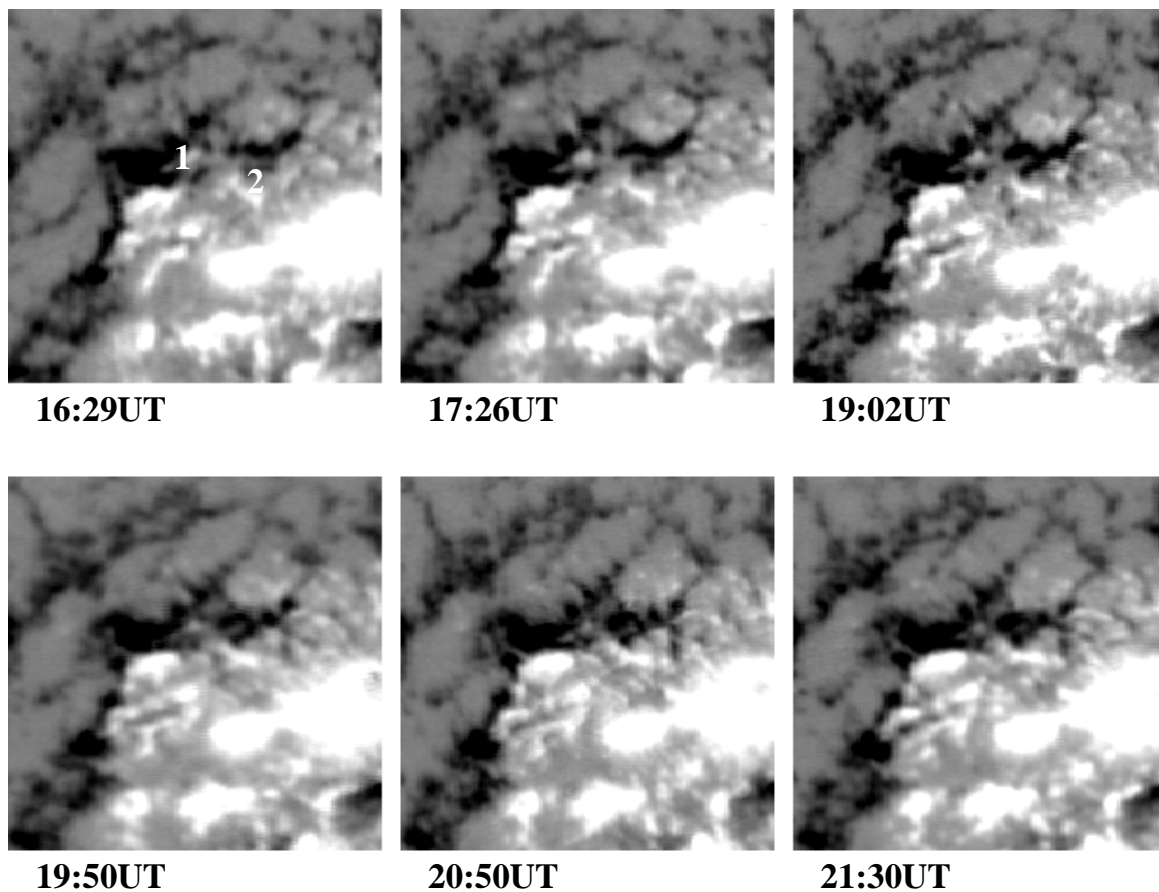


FIG. 12.—Evolution of magnetic fields, showing converging motion and flux cancellation near the contacting point of two loops, which is demonstrated in Fig. 11. Two converging neutral lines are marked “1” and “2.” The field of view is  $100''$  by  $100''$ .

point “X,” where strong magnetic flux cancellation was observed throughout the day. Figure 12 elaborates the detailed evolution of magnetic fields near that point. Rapid converging motions (about  $1 \text{ km s}^{-1}$ ) were detected toward neutral line 2 throughout the observing period. Positive flux in neutral line 1 completely disappeared during the day. However, sudden photospheric magnetic field changes were not detected either around the active regions using high-resolution BBSO data or globally using the lower resolution MDI data. Analyses of several hours of magnetograph data show slow evolution, which is not different from that of a typical nonflare period. Even though we divided the field of view into many small windows, changes in the mean flux density in each window are always below 0.1 gauss, below the noise level of BBSO and MDI magnetograph systems. We were especially careful in examining areas of new coronal holes as a result of dimmings; magnetic changes inside new coronal holes were not detected.

#### 4. DISCUSSION

In many aspects, the two flares presented in this paper are very similar. However, they may represent two different energy release processes: the eruption of twisted loops (1998 April 29 event) and the reconnection of interacting loops (1998 November 5 event). The purpose of this paper is to show that both types of energy release processes may be associated with CMEs. The major morphological difference

is that the former event is associated with the filament eruption, and the later is not. However, it is possible that the November 5 event is associated with an erupting filament that is too hot to be seen in H $\alpha$ . This is unlikely, because no filament was observed in He II  $304 \text{ \AA}$  images either.

Our conclusion that the two flares are physically different is not only based on association with filament eruptions, but also based on the following additional information: the 1998 April 29 event shows a clear S-shaped sheared loop structure, which is a typical sigmoid configuration (Canfield et al. 1999), and the 1998 November 5 event shows two-loop interaction. A separate paper, submitted to *ApJ*, studies this part in detail by using force-free extrapolation, which actually reveals interaction among at least three loops in three different stages (Yurchishin et al. 1999). For the 1998 April 29 event, a sheared magnetic configuration is clearly seen before the flare. Even though we do not know the exact helicity involved, the energy source is clearly released from the single sheared loop. For the 1998 November 5 event, two initial loops appear to be potential. Magnetic reconnection at an interacting point is responsible for release of the energy.

The EUV dimmings are quite obvious in both events. SXT dimmings are hard to detect, probably because of SXT’s dominant sensitivity to higher temperatures. So the lost material may have a relatively lower temperature—about 1.5 million K. Dimmings started 2 hr before flares,

indicating the possibility that the flares and the CMEs are products of a larger scale rearrangement of magnetic structure.

We failed to detect any large-scale or local photospheric magnetic field changes during the flares. Most importantly, no line-of-sight magnetic field changes are detected in the dimming areas. Chromospheric and coronal loop structures are observed to change locally from the more sheared to the more potential form in the flare sites for both events.

We wish to thank the referee, Dr. Richard Harrison, for many valuable comments, which were very helpful in improving the paper. We are grateful to the observing staff at BBSO for their support in obtaining our data. We are also grateful to the *SOHO* team. The work is supported by NSF under grants ATM-9628862, ATM-9714796, and ATM-9713359, by NASA under grants NAG5-4919, NAG5-7350, and NAG5-7085, and by ONR under grant N00014-97-1-1037.

## REFERENCES

- Brueckner, G. E., et al. 1995, *Sol. Phys.*, 162, 357  
 Canfield, R. C., Hudson, H. S., & McKenzie, D. E. 1999, *Geophys. Res. Lett.*, 26, 627  
 Delaboudinière, J. P., et al. 1995, *Sol. Phys.*, 162, 291  
 Domingo, V., Fleck B., & Poland, A. I. 1995, *Sol. Phys.*, 162, 1  
 Feynman, J., & Hundhausen, A. J. 1994, *J. Geophys. Res.*, 99, 8451  
 Gopalswamy, N., & Hanaoka, Y. 1998, *ApJ*, 498, L179  
 Harrison, R. A. 1991, *Philos. Trans. R. Soc. London*, 336, 401  
 ———. 1994, *Adv. Space Res.*, 14, 23  
 ———. 1995, *A&A*, 304, 585  
 ———. 1997, Overview of Results from IACG Campaign 3: CME Onsets (ESA SP-415; Noordwijk: ESA), 121  
 Howard, R. A., Michels, D. J., & Sheeley, N. R., Jr. 1982, *ApJ*, 263, L101  
 McAllister, A. H., Dryer, M., McIntosh, P., Singer, H., & Weiss, L. 1996, *J. Geophys. Res.*, 101, 13  
 Plunkett, S. P., Thompson, B. J., Howard, R. A., Michels, D. J., St. Cyr, O. C., Tappin, S. J., Schwenn, R., & Lamy, P. L. 1998, *Geophys. Res. Lett.*, 25, 2477  
 Scherrer, P. H., et al. 1995, *Sol. Phys.*, 162, 129  
 Sterling, A., & Hudson, H. S. 1997, *ApJ*, 491, L55  
 Thompson, B. J., Plunkett, S. P., Gurman, J. B., Newmark, J. S., St. Cyr, O. C., & Michels, D. J. 1998, *Geophys. Res. Lett.*, 25, 2465  
 Tsuneta et al. 1991, *Sol. Phys.*, 136, 37  
 Verma, V. K. 1990, in *IAU Symp. 142, Basic Plasma Process in the Sun*, ed. E. R. Priest & V. Krishan (Dordrecht: Kluwer), 450  
 Yang, G., & Wang, H. 1999, *BAAS*, 31, 854  
 Yurchishin, V., Wang, H., Qiu, J., Goode, P. R., & Abramenko, V. I. 1999, *ApJ*, submitted  
 Zarro, D. M., Sterling, A. C., Thompson, B. J., Hudson, H. S., & Nitta, N. 1999, *ApJ*, 520, L139